JOURNAL OF THERMOPHYSICS AND HEAT TRANSFER
Vol. 7, No. 3, July–Sept. 1993

Convective Heat Transfer in a Curved Annular-Sector Duct

G. Yang* and M. A. Ebadian†
Florida International University, Miami, Florida 33199

A numerical analysis of heat transfer behavior in a curved annular-sector duct is presented in this article. A uniform axial heat flux and constant peripheral wall temperature boundary condition are applied in this study. The effects of three major parameters on the heat transfer process (the axial pressure gradient, the dimensionless radius ratio, and the dimensionless curvature) are systematically studied. The results indicate that completely different temperature distribution patterns are evident among the segmented duct in different locations relative to the symmetrical centerline. The Nusselt number significantly increases as the pressure gradient increases. Furthermore, an increase of the dimensionless curvature will also enhance heat transfer because of a strong secondary flow. Finally, the results indicate that heat transfer is improved dramatically as the duct radius ratio decreases, especially when the duct radius ratio is smaller than 0.6.

Nomenclature

De = Dean number, $Re(D_h\kappa)^{1/2}$
D_h, d_h = dimensional and dimensionless hydraulic diameter, respectively
(H1) = uniform axial heat flux and peripheral constant wall temperature boundary condition
h = convective heat transfer coefficient, $\mathrm{Wm^{-2}\,K^{-1}}$, Eq. (11)
k = thermal conductivity, $\mathrm{Wm^{-1}\,K^{-1}}$
Nu = Nusselt number, hD_h/k
Pr = Prandtl number, ν/α
p, p^* = dimensionless and dimensional pressures, respectively
Q = function, Eq. (2)
R_i, R_o = inner and outer radius, m, respectively
r, r^* = dimensionless and dimensional radial direction coordinates, respectively
$r^\#$ = radius ratio, R_i/R_o
s, s^* = dimensionless and dimensional axial coordinates, respectively
T, T^* = dimensionless and dimensional temperatures, respectively
T_b, T_b^* = dimensional and dimensionless bulk temperature, respectively
T_w^* = wall temperature, K
u, v, w = dimensionless velocity components $(u^*, v^*, w^*)/(\nu/R_o)$
u^*, v^*, w^* = velocity components in the θ, r, and s directions, $\mathrm{ms^{-1}}$
w_b, w_b^* = dimensionless and dimensional average axial velocities, respectively
X^* = distance to the origin point, Fig. 1
α = thermal diffusivity, $\mathrm{m^2s^{-1}}$
β = function, Eq. (8)
ε = dimensionless curvature, κR_o
θ, θ_0 = angular
κ = curvature, $\mathrm{m^{-1}}$
ν = kinematic viscosity, $\mathrm{m^2s^{-1}}$
ϕ = general variable, Eq. (15)
ω, $\bar{\omega}$ = function, and average of ω, Eqs. (9) and (14), respectively

Introduction

HEAT exchangers in the form of curved ducts are used widely in the food processing, refrigeration, and hydrocarbon industries. The problem of laminar forced convection heat transfer in a curved duct is one of the fundamental problems in convective heat transfer. A recent literature search and publications[1–15] indicate that in recent years much attention has been devoted to the study of curved ducts with different cross sections. In a curved duct, centrifugal force will generate secondary flow in a transverse direction. As a result, the maximum axial velocity will shift toward the outer wall. The higher axial velocity near the outer wall in conjunction with the secondary flow will increase the Nusselt number and the friction coefficient. However, previous studies indicate that the secondary flow pattern depends strongly on the configuration of the cross section of the curved duct. To the authors' knowledge, no investigations on this subject are available in the open literature for a curved annular-sector duct. The major difference between the annular-sector duct and ducts of other geometries discussed before is that the annular-sector duct has both concave and convex boundaries. This study shows that these combined boundaries will significantly affect the secondary flow pattern in the centrifugal force field. The annular-sector duct is often encountered in many compact heat exchangers, i.e, the case of the multipassage, internally finned tube heat exchanger as documented by Soliman[16] and Carnavos.[17] For the straight annular-sector duct, Sparrow et al.[18] analytically obtained the velocity profile, the mean velocity, and the friction factor for fully developed laminar flow. Niida[19] also studied the same problem analytically, and expressed his solution in terms of an equivalent diameter. Soliman[15] further investigated fully developed heat transfer in the straight annular-sector duct with (H1) and (H2) boundary conditions. He tabulated the Nusselt number based on different angle and radius ratios for both boundary conditions.

Unlike the straight duct, the flow and heat transfer behavior in the curved annular-sector duct is sensitive to its location relative to the symmetrical centerline of the holding pipe to which the sector belongs. Figure 1 illustrates the geometry and the toroidal coordinate system for the curved annular-sector duct. The annular-sector duct is bound by an inner wall and an outer wall and two straight walls. If one defines an imagined circle as the holding pipe of the annular-sector duct, the centerline connected between 0–180 deg would be the

---

Received April 15, 1992; revision received Oct. 5, 1992; accepted for publication Oct. 6, 1992.

*Assistant Professor, Department of Mechanical Engineering.

†Professor and Chairman, Department of Mechanical Engineering.

symmetrical centerline. The 0 and 180 deg correspond to the farthest and nearest points, respectively, from the curvature center, 0. The direction of the centrifugal force is 180–0 deg along the symmetrical centerline. In fact, the angle between the annular-sector duct and the symmetry line of the holding pipe can be any value. It is impossible, and also unnecessary, to study all possible curved-sector duct combinations. In this article, only three typical curved annular-sector ducts with a π angle will be discussed, since they represent the predominant behavior of the curved annular-sector duct. To make it easier to describe hereafter, the top segment of the annular-sector duct is defined as 90-0-270 deg, while the bottom and side segments of the duct are defined as 90-180-270 deg and 0-90-180 deg, respectively.

In this article, the heat transfer behavior of hydrodynamically and thermally fully developed laminar flow in a curved annular-sector duct will be discussed. The duct is subjected to the thermal boundary conditions of an axial uniform wall heat flux and a constant peripheral wall temperature, or (H1) boundary condition. The thermal properties of the fluid are considered to be constant, and the viscous dissipation term in the energy equation is assumed to be negligible.

Governing Equation

Figure 1 shows a curved annular-sector duct in the toroidal coordinate system. Assuming a constant curvature κ and introducing the following dimensionless parameters:

$$r = \frac{r^*}{R_o}, \quad s = \frac{s^*}{R_o}, \quad u = \frac{u^* R_o}{\nu}, \quad v = \frac{v^* R_o}{\nu}$$

$$w = \frac{w R_o}{\nu}, \quad p = \frac{p^*}{(\rho^* \nu^2 / R_o^2)}, \quad \varepsilon = \kappa R_o, \quad r^{\#} = \frac{R_i}{R_o}$$

$$D_h = \frac{2\pi(R_o^2 - R_i^2)}{2(R_o - R_i) + \pi(R_o + R_i)}, \quad d_h = \frac{D_h}{R_o} \tag{1}$$

$$De = \frac{\mathrm{d}p^*}{\mathrm{d}s^*} \cdot \frac{R_o^{*3}}{\nu^{*2}\rho^*} (\kappa \cdot R_o)^{1/2} = \frac{\mathrm{d}p}{\mathrm{d}s} \varepsilon^{1/2}$$

$$T = \frac{T^* - T_w^*}{\left(\frac{R_o^2 w_b^*}{\nu}\right)\left(-\frac{\mathrm{d}T_b^*}{\mathrm{d}s^*}\right)}$$

the continuity, momentum, and energy equations governing the fully developed laminar flow in an annular sector within the toroidal coordinate system are given in Eqs. (2–6)[20]

$$\frac{1}{r}\frac{\partial u}{\partial \theta} + \frac{1}{r}\frac{\partial (rv)}{\partial r} = Q \tag{2}$$

$$\frac{1}{r}\frac{\partial (uu)}{\partial \theta} + \frac{1}{r}\frac{\partial (rvu)}{\partial r} = -\frac{1}{r}\frac{\partial p}{\partial \theta} + \frac{\partial^2 u}{\partial r^2} + \frac{1}{r}\frac{\partial u}{\partial r} + \frac{1}{r^2}\frac{\partial^2 u}{\partial \theta^2}$$
$$+ uQ - \frac{vu}{r} + w^2\omega\varepsilon \sin(\theta + \theta_0) + \omega\varepsilon \cos(\theta + \theta_0)\beta$$
$$- \left(\frac{1}{r^2}\frac{\partial^2 u}{\partial \theta^2} + \frac{u}{r^2} + \frac{1}{r}\frac{\partial^2 v}{\partial r \partial \theta} - \frac{1}{r^2}\frac{\partial v}{\partial \theta}\right) \tag{3}$$

$$\frac{1}{r}\frac{\partial (uv)}{\partial \theta} + \frac{1}{r}\frac{\partial (rvv)}{\partial r} = -\frac{\partial p}{\partial r} + \frac{1}{r^2}\frac{\partial^2 v}{\partial \theta^2} + \frac{1}{r}\frac{\partial v}{\partial r} + \frac{\partial^2 v}{\partial r^2}$$
$$+ vQ + \frac{u^2}{r} - w^2\omega\varepsilon \cos(\theta + \theta_0) + \omega\varepsilon \sin(\theta + \theta_0)\beta$$
$$- \left[\frac{1}{r}\frac{\partial v}{\partial r} + \frac{\partial^2 v}{\partial r^2} + \frac{1}{r^2}\frac{\partial^2 (ru)}{\partial \theta \partial r}\right] \tag{4}$$

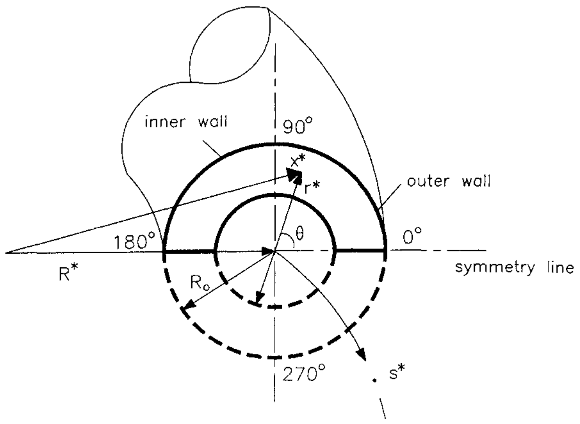

Fig. 1 Geometry and toroidal coordinate system for the curved annular-sector duct.

$$\frac{1}{r}\frac{\partial (uw)}{\partial \theta} + \frac{1}{r}\frac{\partial (rvw)}{\partial r} = -\omega\frac{De}{\sqrt{\varepsilon}} + \frac{1}{r^2}\frac{\partial^2 w}{\partial \theta^2} + \frac{\partial^2 w}{\partial r^2}$$
$$+ \frac{1}{r}\frac{\partial w}{\partial r} + 2wQ + \frac{1}{r}\frac{\partial}{\partial \theta}[w\varepsilon\omega \sin(\theta + \theta_0)]$$
$$- \frac{1}{r}\frac{\partial}{\partial r}[\varepsilon r \omega w \cos(\theta + \theta_0)] \tag{5}$$

where

$$\frac{1}{r}\frac{\partial (uT)}{\partial \theta} + \frac{1}{r}\frac{\partial (rvT)}{\partial r} = \frac{1}{Pr}\left(\frac{1}{r}\frac{\partial^2 T}{\partial \theta} + \frac{\partial^2 T}{\partial r^2} + \frac{1}{r}\frac{\partial T}{\partial r}\right)$$
$$+ TQ + \frac{1}{Pr}\varepsilon\omega\left[\frac{1}{r}\frac{\partial T}{\partial r}\sin(\theta + \theta_0)\right.$$
$$\left. + \frac{1}{r}\frac{\partial T}{\partial \theta}\cos(\theta + \theta_0)\right] + \omega\frac{w}{w_b} \tag{6}$$

$$Q = \varepsilon\omega[-u \sin(\theta + \theta_0) + v \cos(\theta + \theta_0)] \tag{7}$$

$$\beta = \frac{1}{r}\frac{\partial v}{\partial \theta} - \frac{u}{r} - \frac{\partial u}{\partial r} \tag{8}$$

$$\omega = \{1/[1 - \varepsilon r^* \cos(\theta + \theta_0)]\} \tag{9}$$

The θ_0 applied here is used to consider the different orientations of the duct. $\theta_0 = 0$ indicates the top segment of the duct; $\theta_0 = \pi/2$ signifies the side segment of the duct; and $\theta_0 = \pi$ indicates the bottom segment of the duct. The boundary conditions for Eqs. (2–6) will be

$$u = 0, \quad v = 0, \quad w = 0, \quad T = 0 \tag{10}$$

The Nusselt number is defined as

$$Nu = (hD_h/k) = \bar{\omega} Pr d_h^2 / T_b \tag{11}$$

The w_b, T_b, and $\bar{\omega}$ given in Eqs. (2) and (11) are the average axial velocity, bulk temperature, and the average value of ω, respectively, which are defined as

$$w_b = \frac{2}{\pi(1 - r^{\#2})}\int_0^{\pi}\int_{r^{\#}}^{1} wr \,\mathrm{d}r \,\mathrm{d}\theta \tag{12}$$

$$T_b = \frac{2}{\pi w_b (1 - r^{\#2})}\int_0^{\pi}\int_{r^{\#}}^{1} wTr \,\mathrm{d}r \,\mathrm{d}\theta \tag{13}$$

$$\bar{\omega} = \frac{2}{\pi(1 - r^{\#2})}\int_0^{\pi}\int_{r^{\#}}^{1} \omega r \,\mathrm{d}r \,\mathrm{d}\theta \tag{14}$$

Numerical Analysis

The governing equations, Eqs. (2–6), are nonlinear partial differential equations, which are solved by the SIMPLE algorithm.[21] During the calculation, the following convergence criterion is satisfied for all nodes:

$$\frac{\|\phi_{ij}^{k+1} - \phi_{ij}^{k}\|}{\|\phi_{i,j}^{k+1}\|} \le 10^{-5} \tag{15}$$

where ϕ refers to u, v, w, p', and T. Subscripts i and j represent the θ and r coordinates, and superscript k represents the kth iteration. The underrelaxation factors have been applied to obtain a convergent solution. Generally speaking, the greater the Dean number, the smaller the relaxation factor. The relaxation factor ranging from 0.1 to 0.8 has been used according to different computational circumstances.

To assess the accuracy of the governing equations and the validity of the associated computer program, the calculated results have been compared with the bench mark results from Soliman[16] for the case of the straight annular-sector duct. Table 1 indicates that the present prediction agrees very well with the results of Soliman[16]; the maximum differences between the two predictions are less than 1%.

With a 360-deg angle and a zero radius ratio, the annular-sector duct becomes a circular pipe. To verify the accuracy of the computer code, the predicted results for the limited case have been compared with other experimental and numerical predictions. In Fig. 2, the solid line indicates the predicted results by Kalb and Seader,[22] and the solid circles indicate the experimental results from Dravid et al.[23] The open circles represent the prediction from the present analysis, where $Pr = 0.7$ and $\varepsilon = 0.11$ have been applied. Good agreement between these data can be observed from this figure.

Table 1 Comparison of the Nusselt number for the straight annular-sector duct with an angle of 180 deg

$r^{\#} = R_i/R_o$	0.1	0.3	0.5	0.7	0.9
Present study	4.045	4.684	5.601	6.638	7.721
Soliman[16]	4.067	4.639	5.565	6.611	7.691
Deviation	0.30	0.97	0.63	0.42	0.74

Table 2 Effects of the grid size on the fRe, the Dean number, and the fully developed Nusselt number

	$\varepsilon = 0.1(-\mathrm{d}p/\mathrm{d}s) = 20{,}000$ $r^{\#} = 0.7$		$\varepsilon = 0.3(-\mathrm{d}p/\mathrm{d}s) = 20{,}000$ $r^{\#} = 0.5$	
$L \times M$	De	Nu	De	Nu
15 × 15	18.83	6.38	666	18.73
20 × 20	18.74	6.31	672	18.06
30 × 30	18.74	6.26	701	17.07
40 × 40	18.80	6.23	719	16.70
60 × 60	18.96	6.22	746	16.56
80 × 80	19.00	6.22	765	16.62
100 × 100	——	——	765	16.71

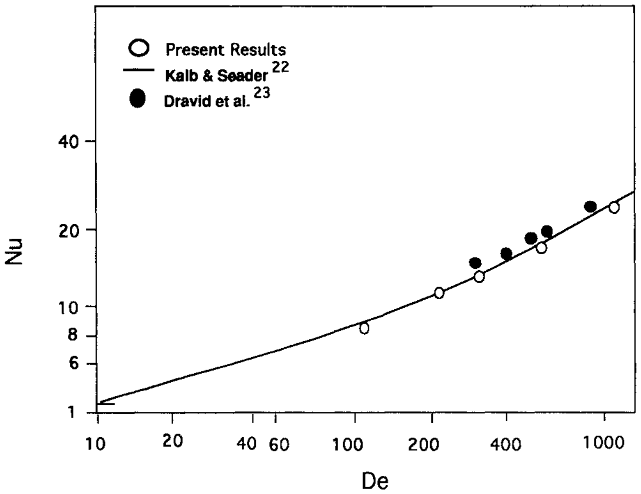

Fig. 2 Comparison of the Nusselt number vs the Dean number ($Pr = 0.7$, $\varepsilon = 0.11$).

Numerical experiments have also been conducted to choose independent grids. Table 2 shows the results of the independent grid study for the two cases with different controlling parameters. The bottom segment duct has been used to conduct the comparison since it provides a more complex flow pattern. The results indicate that fewer grids are needed for the case of a small ε ($\varepsilon = 0.1$). However, a 40 × 40 grid can provide a satisfactory solution, even for the case with a large ε, and the error can be controlled to less than 1%. Therefore, during the calculation, a grid of 40 × 40 was applied.

Results and Discussion

The effects of three major controlling parameters on the heat transfer behavior of the curved annular-sector duct [the axial pressure gradient ($-\mathrm{d}p/\mathrm{d}s$), ε, and $r^{\#}$], will be discussed in this section. The figures in Fig. 3 shows the typical secondary flow pattern and the corresponding dimensionless temperature distribution in the curved annular-sector duct. In Figs. 3b–3d, the left side indicates the flow pattern of the secondary flow, and the right side indicates the contour of the temperature. In these figures, $r^{\#} = 0.5$, $(-\mathrm{d}p/\mathrm{d}s) = 100{,}000$, $\varepsilon = 0.3$ have been applied in the calculations. For purposes of comparison, the temperature distribution for a straight annular duct with $r^{\#} = 0.5$ and $(-\mathrm{d}p/\mathrm{d}s) = 100{,}000$ is also conducted (Fig. 3a). Since the temperature distribution is strongly dependent on the secondary flow, attention is given to the secondary flowfield first. Figure 3b indicates the secondary flow pattern in the top segment of the curved annular-sector duct. Due to the effects of centrifugal force, the fluid along the center of the duct flows upward and induces two vortices on each side of the annular-sector duct (four vortices in the entire domain). The vortex near the outer wall is much stronger than the vortex near the inner wall. Figure 3c shows the secondary flow pattern in the side segment of a curved annular-sector duct. Unlike the top and bottom segments, only two vortices exist in the entire domain in the side segment of the duct. Figure 3d illustrates the secondary flow pattern in the bottom segment of a curved annular-sector duct. Three vortices can be found in each half-domain of the duct. A stronger vortex appears near the outer wall, and the two weaker vortices are near the inner wall. In the region near the symmetrical centerline of the duct, a strong downward flow from the inner wall to the outer wall can be observed in this duct.

Figure 3a shows the dimensionless temperature distribution in a straight annular-sector duct. Since no secondary flow exists, the temperature profiles have crescent shapes, with the high-temperature fluid in the center region and the low temperature fluid near the wall. Figure 3b illustrates the temperature contour of the top segment of the curved annular-sector duct. The downward flow near both the inner and outer solid boundaries moves the low-temperature fluid down to form a low-temperature region in the lower portion of the duct. The upward secondary flow pushes the high-temperature region up and deforms the isothermal contours. Figure 3c illustrates the dimensionless temperature profile for the bottom segment of the curved annular-sector duct. Just as in the top and side segments, the cold fluid flows downward along both solid walls. However, the two streams of downward flow along the inner wall of the duct meet near the centerline, and force the cold fluid to penetrate downward along the centerline. Simultaneously, the two downward flows along the outer wall carry cold fluid upward along the cen-

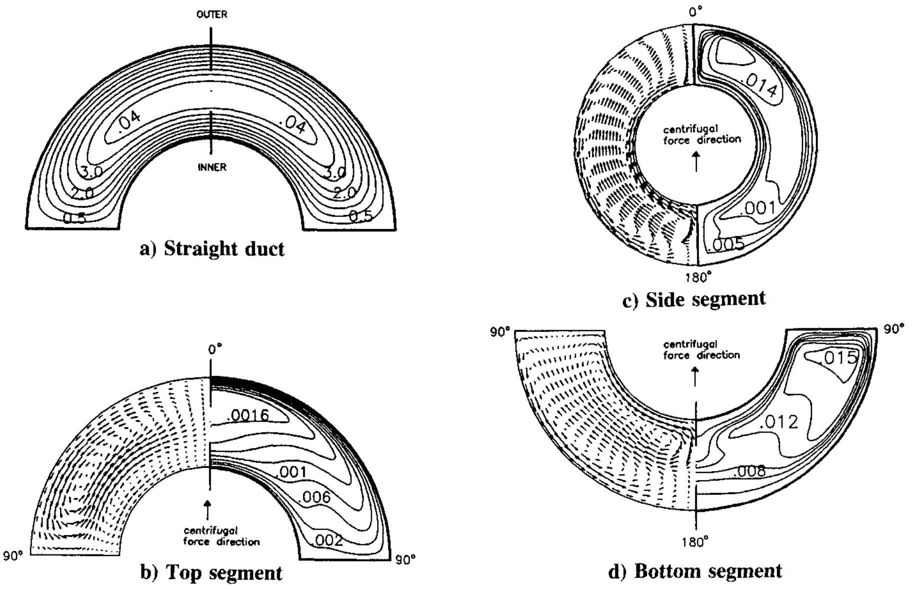

a) Straight duct

c) Side segment

b) Top segment

d) Bottom segment

Fig. 3 Secondary flow and temperature distribution of the curved annular-sector duct ($r^{\#}$ = 0.5, $-dp/ds$ = 100,000, and ε = 0.3).

terline. As a result, the temperature contours are separated into two symmetrical domains. The high-temperature regions are isolated at the top of the duct on each side. In the side segment of the duct, as seen in Fig. 3d, the downward flow pushes the cold fluid to the bottom of the duct, and the high-temperature region can be found in the upper half of the duct.

Figure 4 shows the effect of $r^{\#}$ on the dimensionless temperature distribution. In these figures, the parameters used in the calculation are $\varepsilon = 0.2$ and $-dp/ds = 50{,}000$. Figures 4a–c indicate that the temperature distribution changes with $r^{\#}$ for the top segment of the duct, with the radius ratios of 0, 0.2, and 0.5. When $r^{\#} = 0$, a significant temperature gradient can be seen along the top solid boundary and near the lower boundary, the isothermal line is almost parallel to the solid wall. As $r^{\#}$ increases, the temperature gradient decreases, especially along the lower solid boundary. It is worthwhile to emphasize that unlike the case shown in Fig. 3b, the secondary flow is in a two vortex pattern for the case of $r^{\#} = 0$; that is, there is only one vortex in each half domain. As $r^{\#}$ increases from zero, an additional vortex will be generated along the inner curved surface on each side, as seen in Fig. 3b. The vortices near the inner wall become stronger as $r^{\#}$ increases. These vortices may enlarge the temperature gradient in the region of the lower surface near the symmetrical centerline, but also significantly weaken the temperature gradient in other parts of the lower surface. Figures 4d–f illustrate the temperature contour for the side segment of the curved annular-sector duct. It is worthwhile to emphasize that no matter what $r^{\#}$ is, only a two vortex secondary flow pattern exists for the side segment of the duct. However, as $r^{\#}$ decreases, the secondary flow will become stronger. An explanation for this phenomenon is that the bottom of each isothermal contour is concave for the cases of $r^{\#} = 0$ and $r^{\#} = 0.2$, while the bottom segment of each contour is convex for the case of $r^{\#} = 0.5$. Figures 4g–i illustrate the temperature distribution of the bottom segment of a curved annular-sector duct. As in the top segment, the secondary flow in the bottom segment is in a two-vortex pattern for $r^{\#} = 0$. It may be a four-vortex pattern or six-vortex pattern when $r^{\#}$ is larger than 0. For the two-vortex flow pattern, Fig. 4g shows the temperature contours compress at the top. As $r^{\#}$ increases, the downward and upward cold flows along the inner radius and divides the isothermal contour into two separate peaks, as seen in Figs. 4h and 4i.

Figure 5 illustrates the heat transfer enhancement at different radius ratios of the curved annular-sector duct. The parameters used during the calculation are $\varepsilon = 0.2$ and

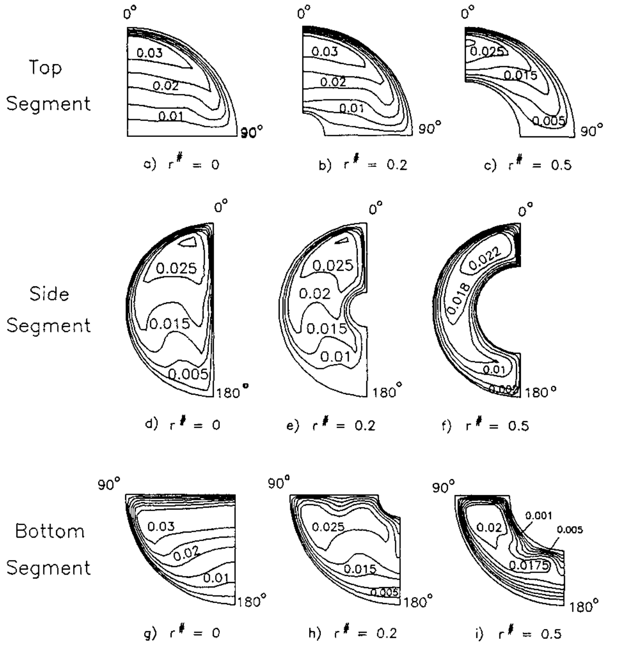

Fig. 4 Effects of the dimensionless radius ratio on the dimensionless temperature distribution (ε = 0.2 and $-dp/ds$ = 50,000).

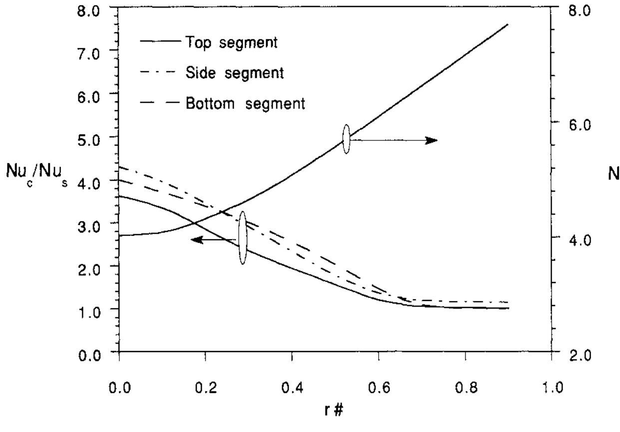

Fig. 5 Effects of the dimensionless radius ratio on the Nusselt number ratio (ε = 0.2 and $-dp/ds$ = 50,000).

$(-dp/ds) = 50{,}000$. It is worthwhile to note that the Nusselt number of the straight annular-sector duct Nu_s is not a constant, but a function of the radius ratio. In order to present the heat transfer enhancement of the curved annular-sector duct, the Nusselt number ratio between the curved annular-sector duct to the straight annular-sector duct is illustrated in this figure, which indicates that the heat transfer enhancement is significantly increased as $r^{\#}$ decreases for all three segments of the duct. For example, when $r^{\#} = 0$, the heat transfer enhancement can reach more than four times that of the higher value $r^{\#}$. When $r^{\#}$ is larger than 0.7, only a minor increase in heat transfer can be found for the curved annular-sector duct. A greater value of $r^{\#}$ signifies that there is a narrow channel between the inner and outer radius walls, making it difficult to generate a strong secondary flowfield. The weaker secondary flow of the $r^{\#}$ with a greater value limits enhancement of heat transfer.

Figure 6 indicates the effects of ε on the thermal behavior of the curved annular-sector duct. The radius ratio of $r^{\#} = 0.5$ and $(-dp/ds) = 20{,}000$ is applied in the calculations. As expected, the Nusselt number increases as ε increases. When $\varepsilon = 0.01$ (which corresponds to a larger curvature radius), the Nusselt number for all three segments is almost the same as that of the straight duct. As ε approaches 0.7, Nu_c/Nu_s approaches 2.37 for the bottom segment of the duct, and 1.35 for the top segment of the duct. Figure 7 shows the temperature distribution affected by the dimensionless curvature at the same controlling parameters as in Fig. 6. In these figures, the left side indicates the temperature contours for the case of $\varepsilon = 0.05$, and the right side indicates the contours for the case of $\varepsilon = 0.5$. Figure 7a shows that the isothermal contours for the top segment of the curved annular-sector duct exhibit the same patterns, that is why the Nusselt number is not sensitive to the increase of ε in the top segment. In Figs. 7b and 7c, the curvature significantly increases the temperature gradient near the solid boundary for the side and bottom segments of the duct compared to the case for the top segment, thus explaining the remarkable heat transfer enhancement found in these two segments.

Figure 8 illustrates the effect of the axial pressure gradient $(-dp/ds)$ on the Nusselt number ratio, Nu_c/Nu_s. The controlling parameters applied to these calculations are $r^{\#} = 0.5$ and $\varepsilon = 0.3$. The pressure gradient is a parameter that controls the axial flow rate. The larger the pressure gradient, the larger the axial flow. There is no significant enhancement of heat transfer at the low flow rate for the curved annular-sector duct until $(-dp/ds)$ reaches 10,000. However, the Nusselt number ratio increases dramatically after the pressure gradient is more than 10,000, thus reflecting the effects of a strong secondary flow. Figure 8 also reveals that the Nusselt number in the bottom segment of the duct is much larger than that in the top segment of the duct, which can be explained by Fig. 3. Comparison of Figs. 3b and 3c indicates that the bottom segment of the curved annular-sector duct has high secondary flows near both inner and outer walls. This high-velocity flow near the solid boundary will significantly reduce the thickness of the thermal boundary layer and result in a significant enhancement of the heat transfer.

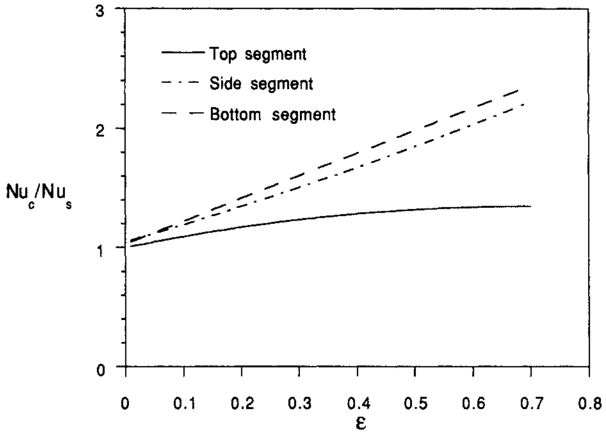

Fig. 6 Effect of the dimensionless curvature on the Nusselt number ratio ($-dp/ds = 20{,}000$, $r^{\#} = 0.5$, and $Nu_s = 5.565$).

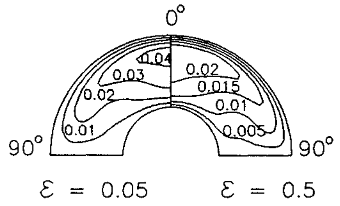

a) Top segment

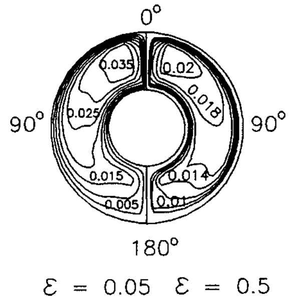

b) Side segment

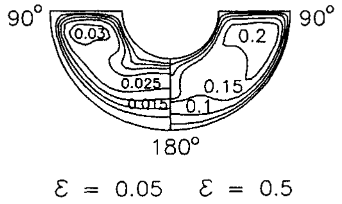

c) Bottom segment

Fig. 7 Effect of the curvature on the dimensionless temperature distribution ($r^{\#} = 0.5$, $-dp/ds = 20{,}000$).

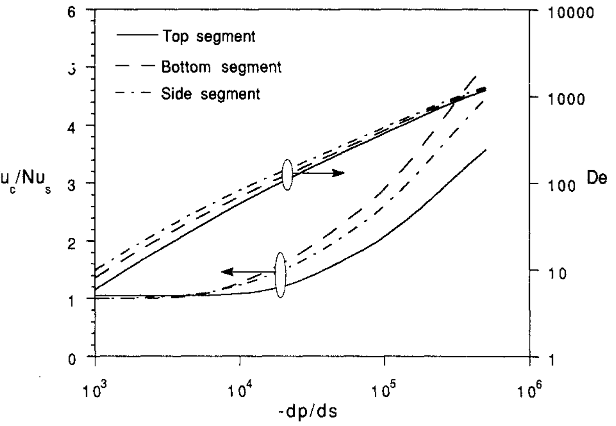

Fig. 8 Effect of the axial pressure gradient on the Nusselt number ratio ($r^{\#} = 0.5$, $\varepsilon = 0.3$, and $Nu_s = 5.565$).

Concluding Remarks

The fully developed thermal heat transfer behavior of the curved annular-sector duct has been discussed in this article. The major findings are as follows:

1) Due to the different secondary flowfields, the dimensionless temperature distribution in three different segments

of the duct exhibits totally different patterns. In the top and side segments of the ducts, the isotemperature contours are deformed and pushed upward, but still maintain a single peak structure. However, for the bottom segment of the curved annular-sector duct, the temperature field is divided into a two-peak structure.

2) Increasing $(-dp/ds)$ can significantly enhance heat transfer for the curved annular-sector duct when the axial pressure gradient is larger than 10^4. The bottom segment of the duct has a higher Nusselt number than the top segment of the duct due to a higher secondary flow velocity in the region of the thermal boundary layer.

3) The Nusselt number increases as ε increases. The bottom segment of the duct reaches the highest value among the three segments, since it experiences a large centrifugal force.

4) Unlike the straight annular-sector duct, the Nusselt number significantly increases as the duct radius ratio decreases for the curved annular-sector duct, especially when $r^\#$ is smaller than 0.6. For a large $r^\#$, only a minor enhancement of heat transfer can be achieved due to the fact that it is difficult to generate a strong secondary flowfield in a narrow channel in the cross section of the duct.

Acknowledgment

The results presented in this article were obtained in the course of research sponsored by the National Science Foundation under Grant CTS-9017732.

References

[1]Akiyama, M., and Cheng, K. C., "Laminar Forced Convection in the Thermal Entrance Region of Curved Pipes with Uniform Wall Temperature," *Canadian Journal of Chemical Engineering*, Vol. 52, 1974, pp. 234–240.

[2]Berger, S. A., Talbot, L., and Yao, L. S., "Flow in Curved Pipes," *Annual Review of Fluid Mechanics*, Vol. 15, 1983, pp. 461–512.

[3]Cheng, K. C., Lin, R. C., and Ou, J. W., "Fully Developed Laminar Flow in Curved Rectangular Channels," *Journal of Fluid Engineering*, Vol. 98, No. 1, 1976, pp. 41–48.

[4]Cheng, K. C., Lin, R. C., and Ou, J. W., "Graetz Problem in Curved Square Channels," *Journal of Heat Transfer*, Vol. 97, No. 2, 1975, pp. 224–248.

[5]Daskopoulus, P., and Lenhoff, A. M., "Flow in Curved Ducts: Bifurcation Structure for Stationary Ducts," *Journal of Fluid Mechanics*, Vol. 203, 1989, pp. 125–148.

[6]Duh, T. Y., and Shih, Y. D., "Fully Developed Flow in Curved Channels of Square Cross Sections Inclined," *Journal of Fluids Engineering*, Vol. 111, 1989, pp. 172–177.

[7]Ghia, K. N., Ghia, U., and Shin, C. T., "Study of Fully Developed Incompressible Flow in Curved Ducts Using a Multi-Grid Technique," *Journal of Fluids Engineering*, Vol. 109, Sept. 1987, pp. 226–236.

[8]Akiyama, M., and Cheng, K. C., "A Graetz Problem in Curved Pipes with Uniform Wall Heat Flux," *Applied Science Research*, Vol. 29, Oct. 1974, pp. 401–418.

[9]Mille, P., Vehrenkamp, R., and Schulz-Dubois, E. O., "The Development and Structure of Primary and Secondary Flow in a Curved Square Duct," *Journal of Fluid Mechanics*, Vol. 151, 1985, pp. 219–241.

[10]Shah, R. K., and Joshi, S. D., "Convective Heat Transfer in Curved Ducts" *Handbook of Single-Phase Convective Heat Transfer*, edited by S. Kakac et al., Wiley, New York, 1987.

[11]Takami, T., and Sudou, K., "Flow Through a Curved Pipe with Elliptic Cross Section," *Bulletin of the Japanese Society of Mechanical Engineers*, Vol. 27, 1984, pp. 1176–1181.

[12]Topakoglu, H. C., and Ebadian, M. A., "On the Steady Laminar Flow of an Incompressible Viscous Fluid in a Curved Pipe and Elliptical Cross Section," *Journal of Fluid Mechanics*, Vol. 158, 1985, pp. 329–340.

[13]Topakoglu, H. C., and Ebadian, M. A., "Viscous Laminar Flow in a Curved Pipe of Elliptical Cross-Section, *Journal of Fluid Mechanics*, Vol. 184, 1987, pp. 571–580.

[14]Thomas, R. M., and Walters, K., "On the Flow of an Elastico-Viscous Liquid in a Curved Pipe of Elliptic Cross Section Under a Pressure Gradient," *Journal of Fluid Mechanics*, Vol. 21, No. 1, 1965, pp. 173–182.

[15]Dong, Z. F., and Ebadian, M. A., "Numerical Analysis of Laminar Flow in Curved Elliptic Duct," American Society of Mechanical Engineers Transactions, *Journal of Fluid Engineering*, Vol. 113, No. 5, 1991, pp. 555–562.

[16]Soliman, H. M., "Laminar Heat Transfer in Annular Sector Ducts," *Journal of Heat Transfer*, Vol. 109, No. 2, 1987, pp. 247–249.

[17]Carnavos, T. C., "Cooling Air in Turbulent Flow with Multi-Passage Internally Finned Tubes," American Society of Mechanical Engineers Paper 78-WA/HT-52, 1978.

[18]Sparrow, E. M., Chen, T. S., and Johnsson, V. K., "Laminar Flow and Pressure Drop in Internally Finned Annular Ducts, *International Journal of Heat and Mass Transfer*, Vol. 7, No. 4, 1964, pp. 583–585.

[19]Niida, T., "Analytical Solution for the Velocity Distribution in Laminar Flow in Annular-Sector Duct," *International Chemical Engineering*, Vol. 20, 1980, pp. 258–265.

[20]Yang, G., and Ebadian, M. A., "Flow Through a Curved Annular Duct," American Society of Mechanical Engineers Transactions, *Journal of Fluid Engineering* (submitted for publication).

[21]Patankar, S. V., *Numerical Heat Transfer and Fluid Flow*, Hemisphere, Washington, DC, 1980.

[22]Kalb, C. E., and Seader, J. D., "Heat and Mass Transfer Phenomena for Viscous Flow in Curved Circular Tubes," *International Journal of Heat and Mass Transfer*, Vol. 15, No. 4, 1972, pp. 801–817.

[23]Dravid, A. N., Smith, K. A., Merrill, E. W., and Brain, P. L. T., "Effect of Secondary Fluid Motion on Laminar Flow Heat Transfer in Helically Coiled Tubes," *American Institute of Chemical Engineers*, Vol. 17, 1971, pp. 1114–1122.